ESRF	**Experiment title:** Establishing a unifying picture of molecular doping of small molecular and polymeric organic semiconductors	**Experiment number**: MA 2463
Beamline: ID10	**Date of experiment**: from: 26.08.2014 to: 02.09.2014	**Date of report**: 25.02.2015
Shifts: 18	**Local contact(s)**: Federico ZONTONE, Oleg KONOVALOV	*Received at ESRF:*

Names and affiliations of applicants (* indicates experimentalists):

***SALZMANN Ingo, 26.08.2014 – 02.09.2014**
Humboldt Universität zu Berlin, Brook-Taylor Straße 6, 12489 Berlin, Germany

***TRUGER Magdalena, 26.08.2014 – 02.09.2014**
Technische Universität Graz, Petersgasse 6, 8010 Graz, Austria

***FRISCH Johannes, 30.08.2014 – 01.09.2014**
HZB, Bereich Solarenergieforschung, Albert-Einstein-Straße 15, 12489 Berlin, Germany

***RÖTHEL, Christian, 26.08.2014 – 02.09.2014**
Technische Universität Graz, Petersgasse 6, 8010 Graz, Austria

***WEGNER, Berthold, 26.08.2014 – 02.09.2014**
Humboldt Universität zu Berlin, Brook-Taylor Straße 6, 12489 Berlin, Germany

***KRIEGNER, Dominik, 26.08.2014 – 02.09.2014**
Charles University, Ke Karlovu 5, 12116 Praha, Czech Republic

Report:

Ground-state integer charge transfer to the dopant is commonly regarded as the basic mechanism of molecular electrical doping in both, conjugated polymers and oligomers. Here, we demonstrate that, on the contrary, fundamentally different processes can occur in the two types of organic semiconductors. Using a number of complementary experimental techniques supported by theory, we contrast polythiophene, where p-doping with a prototypical electron-acceptor leads to integer charge transfer (ICT) reportedly localized to one quaterthiophene (4T) unit on the polymer chain, to the quaterthiophene oligomer itself. Despite a similar increase in conductivity, we observe only partial charge transfer for the latter. In contrast to the parent polymer, pronounced intermolecular frontier-orbital hybridization of oligomer and acceptor in π-stacked 1:1 mixed crystallites, as revealed via grazing-incidence X-ray diffraction (GIXRD) at beamline ID10 at ESRF, leads to the emergence of empty electronic states within the energy gap of the surrounding quaterthiophene matrix. It is the Fermi-Dirac occupation of these gap states that yields free charge carriers and, therefore, the co-crystallites – rather than individual acceptor molecules – should be regarded as the dopants in such systems.

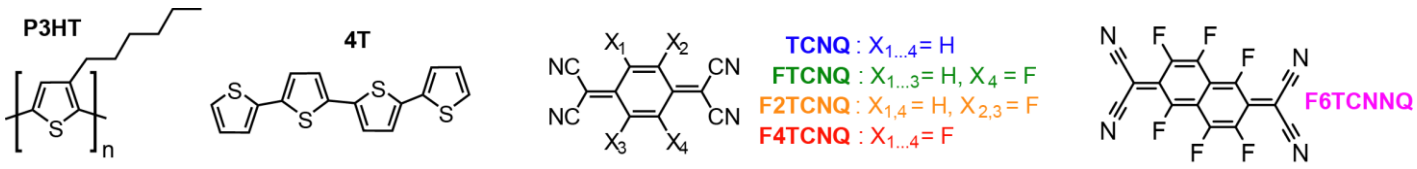

Figure 1: Chemical structures of the materials employed: poly(3-hexylthiophene) (P3HT) and quaterthiophene (4T) as orhganic semiconductors and the increasingly fluorinated tetracyanoquinodimethane (TCNQ) derivatives FTCNQ, F2TCNQ, and F4TCNQ, as well as 2,2'-(perfluoro-naphthalene-2,6-diylidene) dimalononitrile (F6TCNNQ) employed as *p*-dopants.

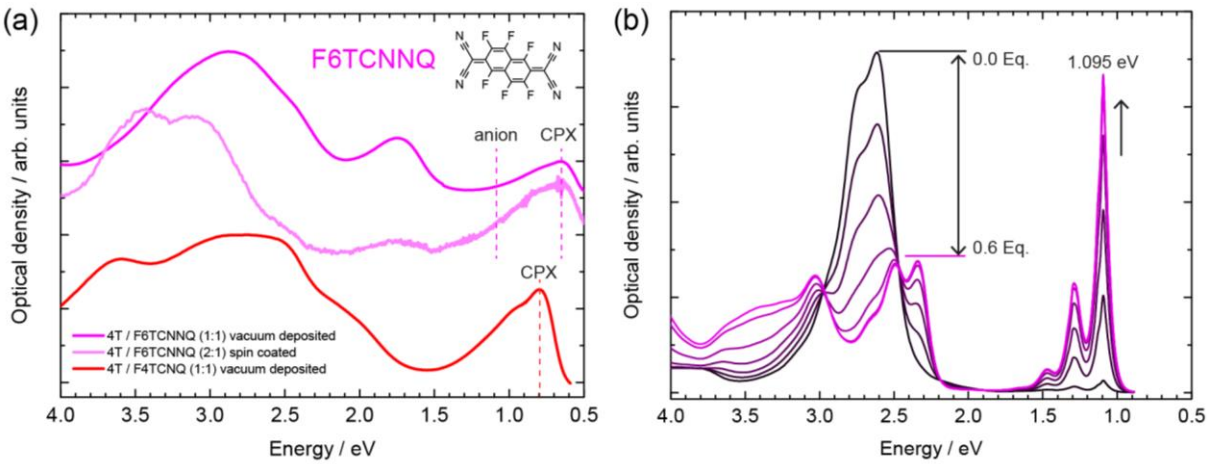

Figure 2: Exemplary UV/Vis/NIR data of 4T/dopant blends and signature of dopant anions. (a) In full analogy to the TCNQ-series, UV/Vis/NIR data on spin coated and vacuum co-deposited blends of 4T with the strongest employed dopant F6TCNNQ [1,2] exhibiting an electron affinity of 5.2 eV [2] shows a new sub-gap absorption that is assigned to the spectral signature of intermolecular frontier-orbital hybridization of oligomer and acceptor upon the formation of a ground-state charge transfer complex (CPX); for comparison, the spectrum of 4T/F4TCNQ is shown (red curve), where the CPX transitions lies higher in energy. In no case, spectral evidence of ionized dopants is observed, which points towards partial instead of integer charge transfer (ICT) upon molecularly doping the thiophene oligomer 4T. (b) Evolution of F6TCNNQ absorption spectra upon titration with increasing equivalents (Eq) of KI in CH_3CN solution yielding radical anions; the lowest energy transition is observed at 1.095 eV; for analogous data on the whole TCNQ series see Ref. [2].

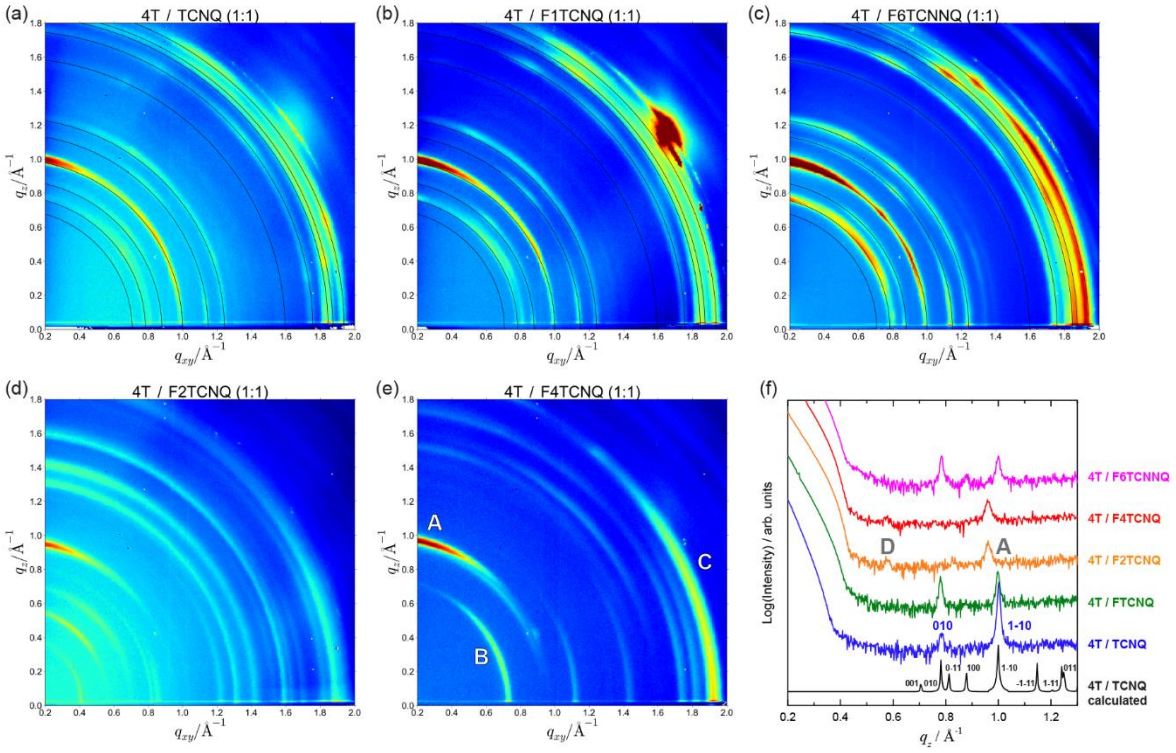

Figure 3: GIXRD and specular XRD data for drop-cast 1:1 blends of 4T with the entire dopant series. (a-e) GIXRD experiments on 4T blends with the whole series of differently strong dopants evidence growth in 1:1 co-crystals of similar structure. From the almost identical patterns (a-c), the 4T/FTCNQ and 4T/F6TCNNQ co-crystals are found to be essentially isostructural to those of 4T/TCNQ, which has been solved by single-crystal X-ray diffraction before (CSD code: FEPYUU) [3]; the strongest reflections calculated for this structure are indicated by black rings. In analogy, the most intense features (labeled as A, B, and C in the preliminary data shown in Figure 4) are also observed in the patterns of 4T/F2TCNQ and 4T/F4TCNQ (d, e) at positions similar to above case, which points towards growth in similar crystal structures. (f) Specular X-ray diffraction data of all 1:1 films as compared to a simulated powder pattern of the known structure of 4T/TCNQ (black curve). For 4T/TCNQ, 4T/FTCNQ, and 4T/F6TCNNQ, the (010) and (1-10) reflections dominate the spectrum, which indicates (some) preferential orientation in the films. Labels A and D correspond to features also observed in the GIXRD data of 4T/F4TCNQ (see Figure 4 below).

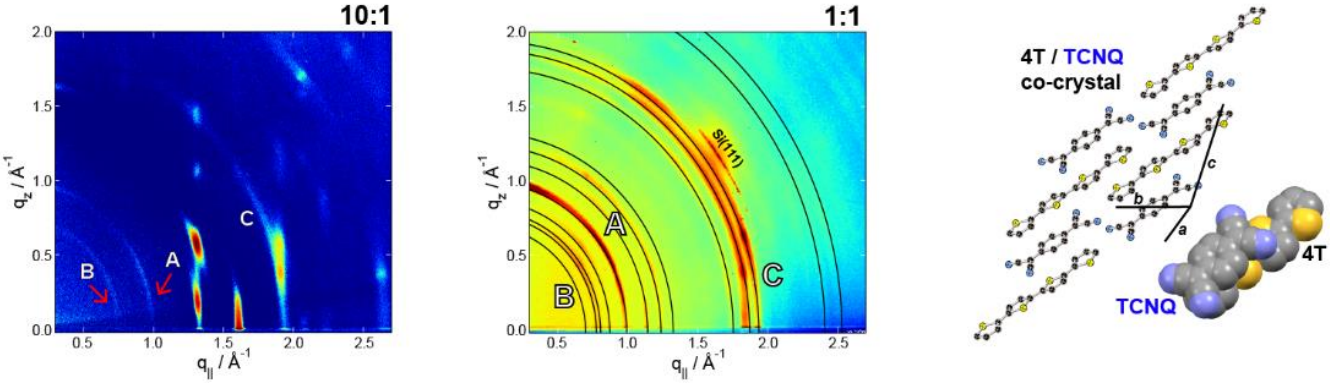

Figure 4: Crystal structure and texture of increasingly doped 4T films. GIXRD data on co-deposited 4T/F4TCNQ films of 10:1 ratio (left), as acquired in preliminary data acquired at HZB. Apart from the vertical Bragg rod corresponding to pure 4T, new features A, B, C were found. These features are assigned to a 1:1 mixed co-crystal structure of 4T/F4TCNQ on the basis of the present experiments at ESRF (middle), as they are likewise found in 1:1 mixed films. This structure is highly similar to a known 4T/TCNQ crystal structure [3] of 1:1 mixed crystals with a coplanarly stacked mutual arrangement of the individual molecules (right). The corresponding calculated reflections are illustrated by black rings in the GIXRD data of a 1:1 co-evaporated 4T/TCNQ reference film (bottom). This very packing motiv induces CPX formation (cf. Figure 2), as the respective frontier molecular orbitals can significantly electronically couple.

This work is submitted for publication as:

Charge transfer in molecularly doped thiophenes: localized or not?

H. Méndez, G. Heimel, S. Winkler, J. Frisch, A. Opitz, K. Sauer, B. Wegner, M. Oehzelt, C. Röthel, S. Duhm, D. Többens, N. Koch, I. Salzmann

---

In a second study carried out at ESRF (ID10), we report on the controlled assembly of the prototypical n-type organic semiconductor N,N'-1H,1H-perfluorobutyl dicyanoperylenecarboxydiimide (PDIF-CN2) into ordered nanoarchitectures and on the multiscale analysis of the correlation between their structural and their electrical properties. By making use of the Langmuir-Blodgett (LB) technique, we formed monolayers of PDIF-CN2 arranged in upright standing molecular packing on different substrates, as evidenced by GIXRD and X-ray reflectivity experiments done at ESRF. Post deposition thermal treatment allowed triggering a reorganization into layered ultrathin crystalline nanostructures, exhibiting structural and photophysical properties similar to those of microscopic crystals obtained by solvent-induced precipitation. The controlled engineering of these molecular architectures on surfaces allowed identifying both a dependence of the monolayer resistance on the

molecular tilt angle in vertical nanojunctions and a pronounced charge-transport anisotropy with enhanced transport along the π-π stacking direction of the PDI core. While a charge carrier mobility for electrons as high as 10^{-2} $cm^2 \cdot V^{-1} \cdot s^{-1}$ was determined in monolayer field-effect transistors for the in-plane direction, being the highest yet reported value for a n-type LB monolayer.

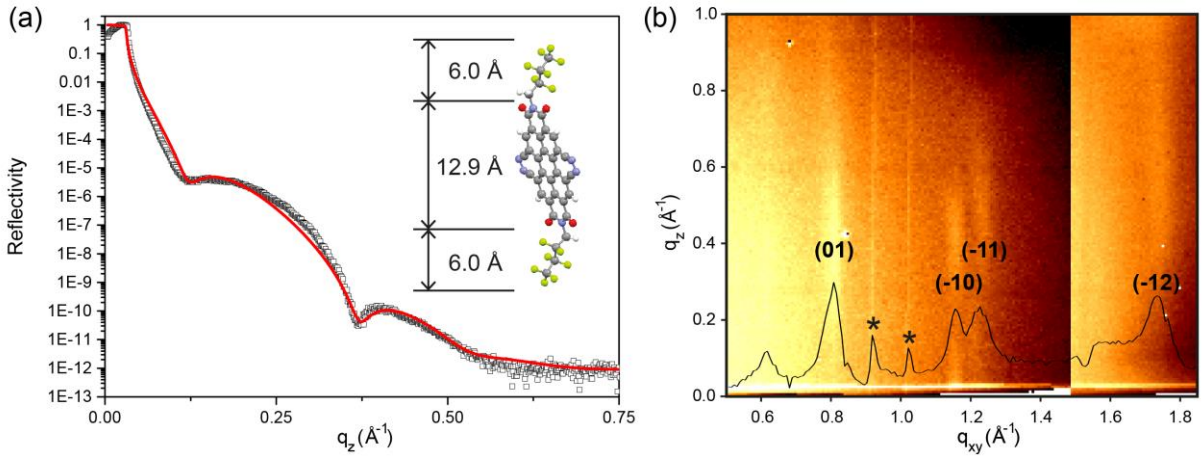

Figure 5: (a) XRR data and best fit (red curve) employing a three-layer model (inset) for the PDIF-CN_2 monolayer on SiO_2. (b) GIXRD reciprocal space map showing diffracted intensity as a function of the components of the scattering vector (q_{xy}, q_z); the black curve represents the diffraction intensity as integrated along q_z for the area shown in the map; stars mark experimental artefacts due to the separated panels of the Pilatus (DECTRIS) detector. The Bragg rods labeled with the respective Miller indices (*h k*) are indicative of two-dimensional crystalline in-plane order of the monolayer; they allow determining the surface unit cell and estimating the backbone tilt angle.

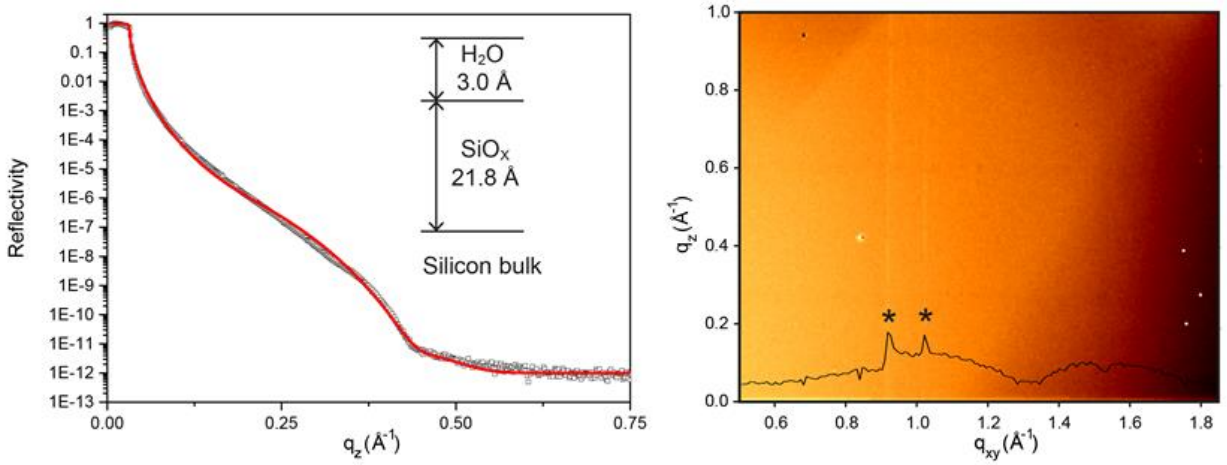

Figure 6: GIXRD reciprocal space map of the bare SiO_2 substrate showing diffracted intensity as a function of the components of the scattering vector (q_{xy}, q_z); the black curve represents the diffraction intensity as integrated along q_z for the area shown in the map; stars mark experimental artefacts.

Table S1: Model parameters of the XRR fit for the PDIF-CN_2 monolayer on SiO_2, as shown in Figure 2a of the main text; *d* denotes the layer thickness, *SLD* the scattering length density at 22 keV primary beam energy, and σ the roughness of the interface. In the XRR fitting procedure, the thickness of the perfluorobutyl regions was fixed to 6.00 Å following recent results of Ringk et al. for a PDI derivative with only a single perfluorobutyl end-substitution [4].

	d / Å	*SLD* / $Å^{-2}$	*σ* / Å
$C_4F_7H_2$	6.0	$1.14 \cdot 10^{-5} + 3.3 \cdot 10^{-7}$i	10.0
$C_{28}N_4O_4H_4$	12.9	$1.00 \cdot 10^{-5} + 2.6 \cdot 10^{-7}$i	4.7
$C_4F_7H_2$	6.0	$1.14 \cdot 10^{-5} + 3.3 \cdot 10^{-7}$i	4.7
SiO_2	2170[a]	$1.89 \cdot 10^{-5} + 3.4\ 10^{-7}$i	6.3
Si bulk	n/a	$2.02 \cdot 10^{-5} + 4.6\ 10^{-7}$i	65.2

[a] *Based on known properties of the substrate (thermally oxidized Si), a starting value of 2100 Å was chosen for the fit.*

To assess the microstructure of the monolayer, we performed X-ray reflectivity (XRR) of the film deposited using the LB technique on SiO_2. Figure 5a shows the experimental data together with a fit employing the Parratt formalism [5] based upon a three-layer model for the organic adsorbate, as illustrated in the inset. Recent XRR data for a self-assembled monolayer of a similar, but only one-end fluorinated PDI-derivative allowed determining the thickness of the perfluorobutyl region to 6.0 Å [4]. By assuming, in analogy, two layers of 6.0 Å above and below the PDI backbone, we find 24.9 Å for the overall thickness of our PDIF-CN_2 monolayer by fitting the XRR data, which is only slightly less than the molecular length indicating (almost) upright standing growth. Since XRR does not allow to draw conclusions on the crystallinity of the layer, we performed GIXRD on the film. The corresponding reciprocal space map is shown in Figure 5b. Clearly, four Bragg rods are observed which indicates that the LB monolayer exhibits lateral crystalline order. The rods are assigned to (01), (-10), (-11), and (-12) in accordance with the strongest reflections of the PDIF-CN_2 single-crystal structure [6]. From the respective in-plane components of the scattering vector (q_{xy}) the surface-unit cell can be refined to $a = 5.61 \pm 0.01$ Å, $b = 8.05 \pm 0.01$ Å, and $\gamma = 104.75 \pm 0.15°$; note that this value of γ equals that of the reported single-crystal structure, while both *a* and *b* are slightly enlarged by ca. 7%. Importantly, the rods observed in GIXRD are not uniform, as would be expected for a monolayer formed by fully upright standing, rod-like molecules [7,8], but show enhanced intensities at values of, e.g., $q_z = 0.4$ $Å^{-1}$ [(10) rod] or at $q_z = 0.6$ $Å^{-1}$ [(-12) rod]. Assuming a similarly π-stacked packing motif as in the single-crystal structure, the structure factor is expected to be particularly high perpendicular to the backbone plane [e.g., (-122) of the single crystal structure]. From the *q*-coordinates of the respective intensity maxima, therefore, the inclination of the molecular backbone with respect to the substrate normal can be estimated to $\mathrm{ArcTan}(q_{xy}/q_z) \approx 20°$. This value is similar to the half of the angle the perfluorobutyl chains are tilted off the PDI backbone plane (44.8°), hence, corroborating the notion of (almost) fully upright-standing molecular growth in the PDIF-CN_2 monolayer.

This work is *accepted* for publication as:

The relationship between structural and electrical characteristics in perylenecarboxydiimide-based nanoarchitectures

C. Musumeci, I. Salzmann, S. Bonacchi, C. Röthel, S. Duhm, N. Koch, P. Samorì

Advanced Functional Materials 2015.

Experimental

Measurements at ID-10 were carried out under Helium flux for sample protection using a three module PILATUS (DECTRIS) area detector for GIXRD and a point detector (scintillator counter) for specular x-ray diffraction. A high primary beam energy of 22 keV [beam geometry (v/h): 0.1/1 mm] was chosen in order to, (i), reduce potential degradation of the organic samples, and (ii), to capture the largest possible q-range ($\Delta q_{xy} \approx 3$ Å^{-1}, $\Delta q_z \approx 2.5$ Å^{-1}) at still reasonable resolution in GIXRD (incident angle of the primary beam: $\alpha_i = 0.064°$ for the SiOx substrates used). The "blind" regions (two vertical lines) of PILATUS due to the three individual modules of the detector were corrected through recording two images sufficiently shifted in q_{xy} direction by default; the individual maps were then joined by a custom-made script finally yielding the full GIXRD data and, furthermore, allowed to judge for sample degradation during the time of exposure to the primary beam (typically 60 sec). Transformation to reciprocal space was done using the software package x-ray utilities [9], which was adapted to the geometry of ID-10 by the first author (D. Kriegner).

References

[1] H. Kleemann, C. Schuenemann, A. A. Zakhidov, M. Riede, B. Lüssem, and K. Leo, Org. Electron. **13**, 58 (2012).
[2] H. Méndez *et al.*, Angew. Chem., Int. Ed. **52**, 7751 (2013).
[3] Q. Minxie, F. Heng, and C. Yong, Chinese Journal of Structural Chemistry **5**, 163 (1986).
[4] A. Ringk *et al.*, Org. Electron. **14**, 1297 (2013).
[5] L. G. Parratt, Physical Review **95**, 359 (1954).
[6] B. A. Jones, M. J. Ahrens, M. H. Yoon, A. Facchetti, T. J. Marks, and M. R. Wasielewski, Angew. Chem. Int. Ed. Engl. **43**, 6363 (2004).
[7] E. C. P. Smits *et al.*, Nature **455**, 956 (2008).
[8] S. C. B. Mannsfeld, A. Virkar, C. Reese, M. F. Toney, and Z. N. Bao, Adv. Mater. **21**, 2294 (2009).
[9] D. Kriegner, E. Wintersberger, and J. Stangl, J. Appl. Crystallogr. **46**, 1162 (2013).